

Biallelic *DMXL2* mutations impair autophagy and cause Ohtahara syndrome with progressive course

Alessandro Esposito^{1,2*}, Antonio Falace^{3*}, Matias Wagner^{4,5,6*}, Moran Gal^{7*}, Davide Mei^{3*}, Valerio Conti³, Tiziana Pisano³, Davide Aprile², Maria Sabina Cerullo^{1,2}, Antonio De Fusco^{1,2}, Silvia Giovedì², Annette Seibt⁸, Daniella Magen^{9,10}, Tilman Polster¹¹, Ayelet Eran^{9,12}, Sarah L. Stenton^{4,5}, Chiara Fiorillo¹³, Sarit Ravid^{9,14}, Ertan Mayatepek⁸, Hava Hafner^{9,15}, Saskia Wortmann^{4,5,16}, Erez Y. Levanon⁷, Carla Marini³, Hanna Mandel^{9,17^}, Fabio Benfenati^{1,18}, Felix Distelmaier^{8^}, Anna Fassio^{2,18^}, and Renzo Guerrini^{3,19^}

¹ Center for Synaptic Neuroscience and Technology, Istituto Italiano di Tecnologia, Genoa, Italy.

² Department of Experimental Medicine, University of Genoa, Genoa, Italy.

³ Pediatric Neurology, Neurogenetics and Neurobiology Unit and Laboratories, Children's Hospital A. Meyer-University of Florence, Florence, Italy.

⁴ Institute of Human Genetics, Klinikum rechts der Isar, Technical University of München, Munich, Germany.

⁵ Institute of Human Genetics, Helmholtz Zentrum München, Neuherberg, Germany.

⁶ Institute for Neurogenomics, Helmholtz Zentrum München, Neuherberg, Germany.

⁷ The Mina and Everard Goodman Faculty of Life Sciences, Bar-Ilan University, Ramat-Gan, Israel.

⁸ Department of General Pediatrics, Neonatology and Pediatric Cardiology, University Children's Hospital Duesseldorf, Medical faculty, Heinrich Heine University, Duesseldorf, Germany.

⁹ Rappaport School of Medicine, Technion, Haifa, Israel.

¹⁰ Pediatric Nephrology Institute, Rambam Health Care Campus, Haifa, Israel.

¹¹ Pediatric Epileptology, Bethel Epilepsy Centre, Bielefeld, Germany.

¹² Department of Radiology, Rambam Health Care Campus, Haifa, Israel.

¹³ Paediatric Neurology and Neuromuscular Disorders Unit, University of Genova and Istituto Giannina Gaslini, Genova, Italy.

¹⁴ Pediatric Neurology Unit and Epilepsy Service, Meyer Children's Hospital, Rambam Health Care Campus, Haifa, Israel.

¹⁵ Neurosurgery laboratory, Rambam Health Care Campus, Haifa, Israel.

¹⁶ Department of Pediatrics, Paracelsus Medical University Salzburg, Salzburg, Austria.

¹⁷ Metabolic Unit, Rambam Health Care Campus, Haifa, Israel.

¹⁸ IRCCS Ospedale Policlinico San Martino, Genoa, Italy.

¹⁹ IRCCS Fondazione Stella Maris, Pisa, Italy.

* These authors contributed equally to this work;

^ These authors contributed equally to this work.

Supplementary case reports

Family 1

Patients 1-II:1 and 1-II:2 were siblings, born to healthy unrelated parents. Both patients were compound heterozygous for the c.5135C>T (p.Ala1712Val) and c.4478C>G (p.Ser1493X) variants.

Patient 1-II:1, a boy, was born at term via eutocic delivery. The Apgar score was 10/10, birth weight 3040 gr (20th percentile), length 49 cm (35th percentile), and OFC 34 cm (20th percentile). At birth, sub-continuous seizures with tonic contractions and clonic jerks with multifocal distribution or involving the four limbs were noted, lasting 30-40 seconds. EEG recordings showed a burst suppression pattern since the first days of life, associated with multifocal spikes. During the first year of life, tonic spasms became the prominent seizure type, with multiple daily episodes, at times in series. Various trials with different medications, including pyridoxine, pyridoxal-phosphate, biotin, phenobarbital, phenytoin, folic acid, levetiracetam, and midazolam, lorazepam, vigabatrin, failed to reduce seizures in the first months of life. Adrenocorticotrophic hormone (ACTH) transiently controlled seizures. Brain MRI, performed at birth and repeated at 2 and 16 months, revealed thin corpus callosum, hypomyelination and subsequent leucoencephalopathy, with mild atrophy. MRI spectroscopy revealed metabolite values consistent with severe brain dysmaturity and reduced neuronal pool (white matter: NAA/Cr, 0.87, Cho/Cr 1.19, Cho/NAA 1.36; basal ganglia NAA/Cr 0.67, Cho/Cr 1.02, Cho/NAA 1.52; brainstem NAA/Cr 1.06, Cho/Cr 1.41, Cho/NAA 1.33). Throughout follow-up the child exhibited severe hypotonia, quadriplegia, absence of spontaneous movements, no eye tracking, and acquired no milestones. Minor dysmorphic facial features were noted, including mild downslanting of palpebral fissures, epicanthal folds, short forehead, saddle nose, myopathic facies, and high arched palate. Head size at four years was 45 cm (<1st centile, -3.6 SD). Brainstem evoked response audiometry (BERA) screening indicated bilaterally impaired conduction. Nerve conduction study (NCS) revealed mild peripheral polyneuropathy. Muscle biopsy showed a fairly normal muscle tissue, without ragged red fibre, with normal fibre type distribution, and abundant lipid droplets visible in several muscle cells. Laboratory work-up including screening for metabolic diseases was normal. The child died at four years due to respiratory complications of the severe neurological condition.

Patient 1-II:2, a girl, was born at term via eutocic delivery. The Apgar score was 10/10, birth weight was 2700 gr (9th percentile), length was 49 cm (45th percentile), and OFC was 34 cm (29th percentile). At birth, eyelid fluttering, eyes deviation, and oroalimentary automatisms, were followed by sub-continuous, migrating, focal clonic polymorphic seizures and tonic spasms. EEG recordings showed a burst suppression pattern and multifocal spikes. Pyridoxine, pyridoxal-phosphate, biotin, folic acid, phenobarbital, ACTH, and midazolam had no effect on seizures. Potassium bromide treatment resulted in transient seizure reduction. Brain MRI at birth revealed a thin corpus callosum. Neurological development was profoundly impaired, with severe hypotonia, quadriplegia, absence of spontaneous movements and no eye tracking. Minor dysmorphic facial features were noted, including mild downslanting of palpebral fissures, epicanthal folds, short forehead, saddle nose, myopathic facies, high arched palate. Clinical examination also revealed non-pitting oedema of limbs, and pubic hair growth with normal endocrine profile. Head size at four years was 44 cm (<1st centile, -3.6 SD). At five years, tonic spasms became more frequent and

intense, accompanied by cyanosis. BERA screening indicated bilateral sensorineural hearing loss. NCS revealed mild peripheral polyneuropathy. Laboratory work-up, including screening for metabolic diseases was normal. The child died at five years ten months due to complications of the severe neurological condition.

Family 2

Patients 2-II:1 and 2-II:2 were born to 1st degree Israeli Arab cousins. Both patients were homozygous for the c.4478C>A (p.Ser1493X) variant.

Patient 2-II:1, a boy, was born at term after an uncomplicated pregnancy via caesarean section. The Apgar score was 9/9, birth weight was 3200 gr (25th percentile), and OFC was 38 cm (90th percentile). At birth, the patient presented with myoclonic seizures treated with phenobarbital, but proving resistant to medication. Repeated EEGs showed multifocal and generalized epileptiform discharges and discontinuous background with burst suppression. Brain MRI, performed at five months, revealed thin corpus callosum, hypomyelination, mild cortical atrophy, and dilated ventricles. At clinical examination, the child exhibited early severe hypotonia, no spontaneous movements, no acquired developmental milestones, no eye tracking, and no response to stimuli. Dysmorphic features were noted, including dolichocephaly, slight downslanting of palpebral fissures, epicanthal folds, short forehead, saddle nose, myopathic facies, high arched palate, and non-pitting oedema of limbs. BERA analysis indicated sensorineural hearing loss and NCS revealed a peripheral polyneuropathy. Head size at one year was 47.3 cm (69th centile). Extensive biochemical and metabolic studies, including complete blood count, renal, liver, muscle, and thyroid function were normal. CSF glucose, protein, amino acids and lactate, and plasma lactate, amino acids, ammonia, very-long-chain fatty-acids, phytanic and pristanic acid, isoelectric focusing of transferrin, acyl-carnitine in dry blood spot and urinary amino and organic acids profiles were unremarkable. Lysosomal storage diseases, including GM1 gangliosidosis, MLD, Hex A+B deficiency, and Krabbe disease were also excluded. The patient died at 19 months following aspiration pneumonia.

Patient 2-II:2, a girl, was born at 35 weeks of gestation via caesarean section due to polyhydramnios and hydrops fetalis. The Apgar score was 2/4, birth weight was 3085 gr (90th percentile), and OFC was 39 cm (>99th percentile = +2.3 SD). After birth, she required resuscitation and mechanical ventilation for 24 hours. As observed in her brother, at birth, myoclonic seizures occurred in clusters and were refractory to multiple antiepileptic drugs. Repeated EEGs showed disorganized background with multifocal generalized epileptic discharge and a burst suppression pattern. Brain MRI at three months revealed thin corpus callosum with hypomyelination. A second MRI scan, at age 2 years, additionally showed leucoencephalopathy with cortical atrophy and dilated ventricles. At clinical examination, the girl exhibited severe hypotonia, no spontaneous movements, no milestones acquired, no eye tracking, and no response to external stimuli. Dysmorphic features were noted, including slight downslanting of the palpebral fissures, epicanthal folds, short forehead, saddle nose, myopathic facies, high arched palate, dolichocephaly non-pitting oedema of limbs, obesity, and hirsutism. Erratic eye movements with normal appearing retinas were documented. BERA analysis indicated severe bilateral sensorineural hearing impairment. NCS indicated peripheral polyneuropathy. No visual evoked potentials (VEPs) nor retinal short and medium

latency responses could be elicited. Head size at one year was 49 cm (>99th centile = +3SD). Extensive biochemical and metabolic studies including complete blood count, renal, liver, muscle, and thyroid function were normal. CSF glucose, protein, amino acids and lactate, and plasma lactate, amino acids, ammonia, very-long-chain fatty-acids, phytanic and pristanic acid, isoelectric focusing of transferrin, acyl-carnitine in dry blood spot and urinary amino and organic acids profiles were unremarkable. Lysosomal storage diseases, including GM1 gangliosidosis, MLD, Hex A+B deficiency, and Krabbe disease were also excluded. Endocrinological studies performed at age 8.5 years ruled out recurrent episodes of hypoglycaemia. HbA1C, TSH, and FT4 were normal. The patient underwent gastrostomy at age 6 weeks and tracheostomy at age 6 years to prevent repeated hospital admissions due to aspiration pneumonia. She died at nine years due to respiratory complications of the severe neurological condition.

Family 3

Patients 3-II:4 and 3-II:5 were born to 1st degree Turkish cousins. Both patients were homozygous for the c.7518-1G>A (p.Trp2507ArgfsX4) variant.

Patient 3-II:4, a boy, was born at 38 weeks gestation, after an uneventful pregnancy via caesarean section, due to breech position. The Apgar score was 6/7, birth weight was 2980 gr (35th centile), length was 49 cm (45th centile), and OFC was 35 cm (77th percentile). At birth, the child was transferred to the intensive care unit due to respiratory distress. From the second day of life, frequent tonic and myoclonic seizures were observed. EEG showed a burst suppression pattern. Initial antiepileptic therapy using vitamin B6, phenobarbital and sulthiame was ineffective. During the following months, the child experienced multiple seizures per day in spite of various antiepileptic drug regimens, including levetiracetam, valproate, vigabatrin, zonisamide, and midazolam, given as continuous infusion. Steroids were also ineffective. Brain MRI, at one month, revealed thin corpus callosum and a simplified gyral pattern, with normal cortical thickness, in both frontal lobes. A repeat brain MRI at 10 months, also revealed hypomyelination, symmetrical leukoencephalopathy, and cerebellar and brainstem atrophy. At clinical examination, the boy exhibited severe hypotonia, no spontaneous movements, no milestones acquired, profound ID, no eye tracking, and dysmorphic features, including slight downslanting of palpebral fissures and epicanthal folds. BERA indicated bilateral hearing impairment. Head size at 10 months was 50 cm (>99th centile, +3.1SD). Further diagnostic work-up (laboratory analysis of blood, urine and CSF, metabolic investigations, chromosomal analysis, eye examination, etc.) was unrevealing. Oral feeding was not possible and a PEG tube was placed. The further clinical course was complicated by intractable seizures. The patient died at 3 years due to complications of the severe neurological condition.

Patient 3-II:5, a girl, was born via caesarean section, at 32 weeks gestation, due to pathological cardiotocography (CTG). The Apgar score was 4/6, birth weight was 1890 gr (72nd percentile), length was 43.5 cm (80th percentile), and OFC was 30 cm (78th percentile). Soon after birth she developed severe respiratory distress requiring mechanical ventilation for six days. In the following days the condition of the child stabilized but frequent tonic spasms appeared. Initial EEG recordings showed a burst suppression pattern comparable to that observed in her brother. Antiepileptic treatment using vigabatrin slightly reduced seizure frequency. During the following months, the

clinical conditions of the child remained relatively stable. Brain MRI at one month revealed thin corpus callosum and a diffusely simplified gyral pattern, without cortical thickening, more prominent in the frontal lobes. At clinical examination the patient exhibited early severe hypotonia, no spontaneous movements, no milestones acquired, no eye tracking, and dysmorphic features, including slight downslanting of palpebral fissures, epicanthal folds. Mild pubic hair growth was noted around the age of 7 months, without breast development or clinical features of virilization. DHEA-S (42 μ g/dl; normal < 124 μ g/dl) and testosterone (< 0,07ng/ml; normal <0.2 ng/dl) were unremarkable. Luteinizing hormone (0.8 mIU/ml; normal < 4 mIU/ml), follicle-stimulating hormone (5.2 mIU/ml; normal range 0.1-6.0 mIU/ml), oestradiol (15 pg/ml, normal range 7-40pg/ml), IGF1 (208.6 ng/ml; 50.-95. percentile) were normal. IgF-BP3 (3.56 mg/l; 97.5 percentile = 3.5ng/ml) was slightly elevated. Thyroid hormones and cortisol levels were normal. Blood sugar levels were repeatedly normal. Laboratory work-up including screening for metabolic diseases was normal. BERA screening indicated hearing impairment. At last follow-up, at age 10 months, the patient still exhibits frequent tonic seizures (> 10/day) and shows no developmental progress.

Supplementary Methods

Whole-exome sequencing and data analysis

Family 1

DNA library preparation and whole-exome enrichment was performed in three individuals (1-I:1, 1-I:2, and 1-II:2, Fig. 1A) using the SureSelect Human All Exon v4 (Agilent Technologies, Santa Clara, CA). Captured Libraries were sequenced on an Illumina HiSeq 2000 according to the 2x90bp paired-end read sequencing protocol (Illumina, San Diego, CA). Sequencing reads passing quality filtering were aligned to the human genome assembly (hg19) with Burrows-Wheeler Aligner (BWA) (Li et al., 2010). The Genome Analysis Toolkit (GATK) (McKenna, et al., 2010) was used for base quality score recalibration, indel realignment, duplicate removal, and to perform single nucleotide variants (SNVs) and small insertions and deletions (INDELs) discovery and genotyping across all samples simultaneously using variant quality score recalibration according to GATK Best Practices recommendations (DePristo et al., 2011; Van der Auwera et al., 2013). Samples had a mean depth of target region covered at 64.1X and 96.93% of bases in the consensus coding sequences (CCDS) covered by at least 10 reads. For annotating and filtering data, we used the VarSeq tool (Golden Helix, Bozeman, MT).

We analysed homozygous recessive and compound heterozygous models using the VarSeq tool, incorporating the annotated variant data and pedigree information. Although pedigree analysis in this non-consanguineous family was suggestive of a recessive phenotype, we considered the possibility of parental gonadal mosaicism and also applied the *de novo* model. Variants with depth <10, with a minor allele frequency (MAF) >2% or for which more than 5 homozygous/hemizygous individuals were reported in the genome aggregation database (gnomAD), were filtered out. Variants predicted to alter protein function (non-synonymous, stop-gain, stop-loss, frameshift, and splice-junction mutations) were submitted for validation and segregation testing by Sanger sequencing in the proband (1-II:1).

Family 2

We collected genomic DNA samples from both affected children (2-II:1 and 2-II:2), their parents (2-I:1 and 2-I:2) and healthy siblings (2-II:3, 2-II:4 and 2-II:5) (Fig. 1A). Whole-exome was enriched in individual 2-II:2 using the NimbleGen SeqCap EZ exome 44M kit and sequenced on a Illumina HiSeq 2000 using a 2x100bp paired-end read protocol (BGI, Shenzhen, China). About 87 million paired-end reads were generated and aligned to the human genome assembly hg19 using the Burrows-Wheeler Alignment tool version 0.6.1 (Li & Durbin 2009), and duplicates were removed with PICARD (Li et al., 2009). Samples had a mean depth of target region covered at 153X with 98% of bases covered by at least 10 reads.

Variants were called with GATK toolkit version 1.6-7 (McKenna et al., 2010) and annotated using ANNOVAR (Wang, et al., 2010). Linkage analysis to extract the homozygous regions from WES data was performed with the LINKDATAGEN software (Smith et al., 2011) and the MERLIN linkage software (Abecasis et al., 2002). The genetic model assumed for linkage analysis was fully penetrant recessive disease with a population disease allele frequency of 0.00001. The LOD scores were estimated at positions spaced 0.3-cM apart, and CEU allele frequencies were used. A cut-off of LOD score >1 was used to define homozygous linked genomic regions. After retaining only variants lying within those homozygous regions, the list was further filtered to exclude variants that are present in any of the public human variation databases (dbSNP130, 1000G, and NHLBI-ESP) at a frequency of at least 0.01. Variants resulting in synonymous changes or those called as heterozygotes were removed. Filtering steps reduced the candidate genes list to 23 variants that were manually reviewed using Integrative Genomic Viewer (IGV, Thorvaldsdóttir et al., 2013) and studied for their potential involvement in the observed phenotype.

Family 3

Genomic DNA samples were collected from both parents (3-I:1 and 3-I:2) and affected siblings (3-II:4 and 3-II:5) (Fig. 1A). Whole-exome sequencing was performed in three individuals (3-I:1, 3-I:2 and 3-II:5) as previously described (Kremer et al., 2017).

In brief, trio exome sequencing was performed using Sure Select Human All Exon kit V6 (Agilent, Santa Clara, CA) for exome enrichment and a HiSeq4000 system (Illumina, San Diego, CA) for sequencing. The average read depth was 129X. Reads were aligned to the human genome assembly (hg19) with Burrows-Wheeler algorithm (BWA v.0.5.9, Li & Durbin 2009). More than 98% of the target sequences were covered at least 20X. SNVs as well as INDELs were detected with SAMtools v.0.1.19 (Li et al., 2009). In-house custom Perl scripts were used for variant annotation. Based on the high likelihood of recessive inheritance and parental consanguinity, we filtered data for homozygous variants with a minor allele frequency <0.1% in our in-house database with 15,000 individuals and identified 22 variants.

***DMXL2* Sanger sequencing validation and segregation analysis**

Primer sequences used for validations and segregations analyses are reported in Supplementary Table 2.

Family 1

DMXL2 exons 18 and 22 were PCR amplified in individuals 1-I:1, 1-I:2, 1-II:1 and 1-II:2 with an annealing temperature of 60°C and an extension time of 1 min using the FastStart Taq DNA

Polymerase (Sigma-Aldrich, St. Louis, MO). PCR products were cycle sequenced on both strands using the BigDye Terminator v 3.1 chemistry (Thermo Fisher Scientific, MA) and run on a 3500DX genetic analyzer (Thermo Fisher Scientific).

Family 2

DMXL2 exon 18 was PCR amplified in individuals 2-I:1, 2-I:2, 2-II:1, 2-II:2, 2-II:3, 2-II:4 and 2-II:5 with a standard PCR protocol. PCR products were cycle sequenced on both strands using the BigDye Terminator v 3.1 chemistry (Thermo Fisher Scientific) and run on a 3730XL genetic analyzer (Applied Biosystems, Warrington, UK).

Family 3

DMXL2 exon 31 was PCR amplified in individuals 3-I:1, 3-I:2, 3-II:4 and 3-II:5 with a touchdown PCR protocol (annealing temperature from 65°C to 54°C) and an extension time of 30 sec using the HotStarTaq Plus DNA Polymerase (Qiagen, Hilden, Germany). PCR products were cycle sequenced on both strands using the BigDye Terminator v 3.1 chemistry (Thermo Fisher Scientific) and run on a 3730XL genetic analyzer (Thermo Fisher Scientific).

Supplementary Table 1: *in silico* predictions and annotations

Variant	Genomic Location (Hg19)	Reference allele	Alternative allele	Consequence	Gene	RefSeq accession	EXON	INTRON	Protein	gnomAD exomes Allele Frequency	gnomAD genomes Allele Frequency
1	15:51757849	C	T	splice_acceptor_variant	DMXL2	NM_015263.3	-	30/42	-	-	-
2	15:51780233	G	A	missense_variant	DMXL2	NM_015263.3	22/43	-	A1712V	-	-
3	15:51790943	G	C	stop_gained	DMXL2	NM_015263.3	18/43	-	S1493*	-	-
4	15:51790943	G	T	stop_gained	DMXL2	NM_015263.3	18/43	-	S1493*	-	-
Variant	REVEL score	M-CAP pred	Eigen PC phred	DANN score	ada score	rf score	dpsi zscore	CADD phred	MutationAssessor pred	MutationTaster pred	SIFT pred
1	-	-	-	-	0.999	0.94	-3.39	-	-	-	-
2	0.8	D	14.74	0.999	-	-	-	33	H	D	D
3	-	-	23.16	0.996	-	-	-	39	-	A	-
4	-	-	14.59	0.996	-	-	-	40	-	A	-
Variant	GenoCanyon score	VEST3 score	FATHMM pred	fathmm-MKL coding pred	GERP++ RS	Interpro domain	MetaLR pred	MetaSVM pred	LRT pred	PROVEAN pred	phastCons100way vertebrate
1	-	-	-	-	-	-	-	-	-	-	-
2	1	0.892	T	D	4.97	Rav1p_C	D	D	D	D	1
3	1	-	-	D	5.61	WD40/YVTN_repeat	-	-	D	-	1
4	1	-	-	D	5.61	WD40/YVTN_repeat	-	-	D	-	1
Variant	Polyphen2 HDIV pred	Polyphen2 HVAR pred	phyloP20way mammalian	phastCons20way mammalian							
1	-	-	-	-							
2	D	D	0.998	0.993							
3	-	-	0.998	1							
4	-	-	0.998	1							

Table legend: Hg19: Human Genome hg19 assembly; -: missing/not available value; D: damaging; H: high impact; T: tolerated; A: disease causing automatic; pred: prediction

Cut-offs considered as significatives for continuous values: p-value REVEL > 0.5; Eigen PC phred > 10; p-value DANN score > 0.8; p-value ada and rf score (dbSNV) > 0.6;

dpsi zscore (SPIDEX) < -2; CADD phred > 20; p-value VEST3 score > 0.7; GERP++ RS > 4 (conserved); p-value phyloP20way mammalian, phastCons100way vertebrate, phastCons100way vertebrate and phastCons20way mammalian > 0.8 (conserved)

see the following references for additional information about the tools used in the table:

(dbSNFP) Liu, X. *et al.* dbSNFP v3.0: A One-Stop Database of Functional Predictions and Annotations for Human Nonsynonymous and Splice-Site SNVs. *Hum. Mutat.* 2016; 37: 235–41

(REVEL) Ioannidis, N. M. *et al.* REVEL: An Ensemble Method for Predicting the Pathogenicity of Rare Missense Variants. *Am. J. Hum. Genet.* 2016; 99: 877–85

(M-CAP) Jagadeesh, K. A. *et al.* M-CAP eliminates a majority of variants of uncertain significance in clinical exomes at high sensitivity. *Nat. Genet.* 2016; 48: 1581–6

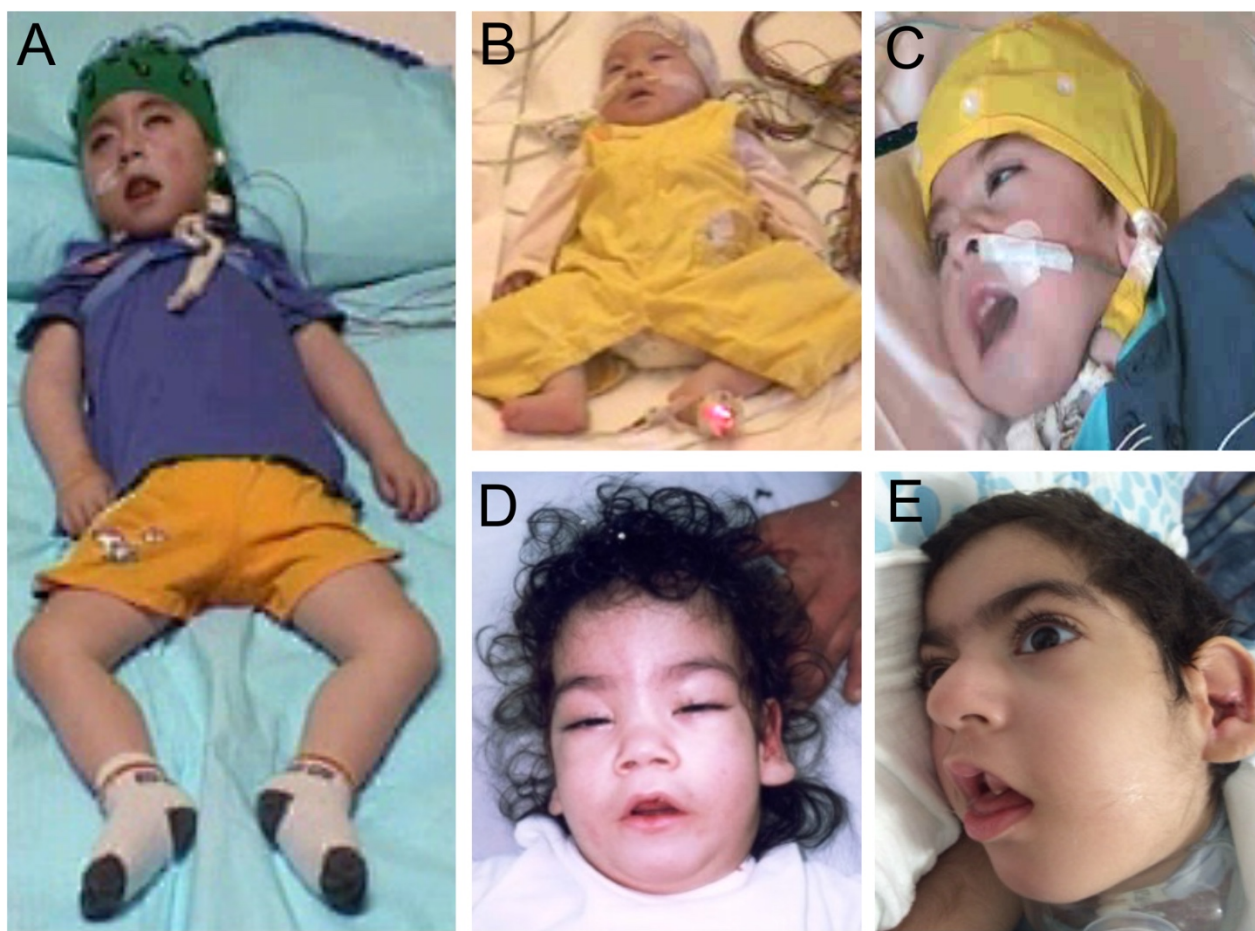
(EIGEN) Ionita-Laza, I *et al.* A spectral approach integrating functional genomic annotations for coding and noncoding variants. *Nat. Genet.* 2016; 48: 214–20

(dbSNV) Jian, X. & Liu, X. In Silico Prediction of Deleteriousness for Nonsynonymous and Splice-Altering Single Nucleotide Variants in the Human Genome. *Methods Mol. Biol.* 2017; 1498: 191–7

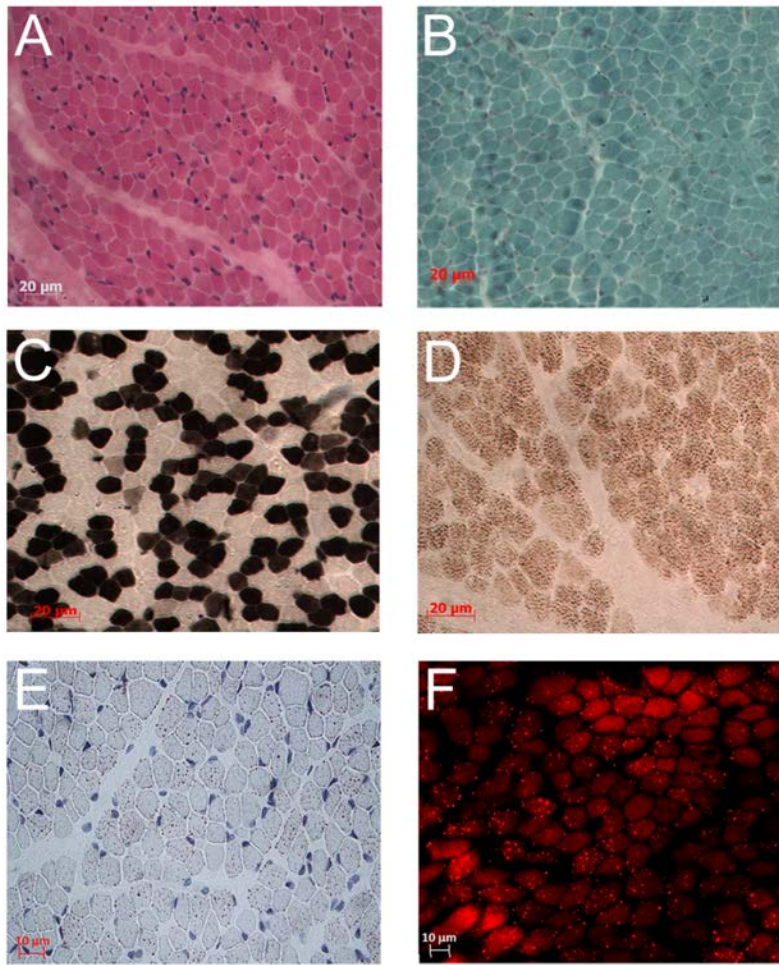
(SPIDEX) Xiong, H. Y. *et al.* RNA splicing. The human splicing code reveals new insights into the genetic determinants of disease. *Science* 2015; 347: 1254806

Supplementary Table 2. Primers for Sanger sequencing

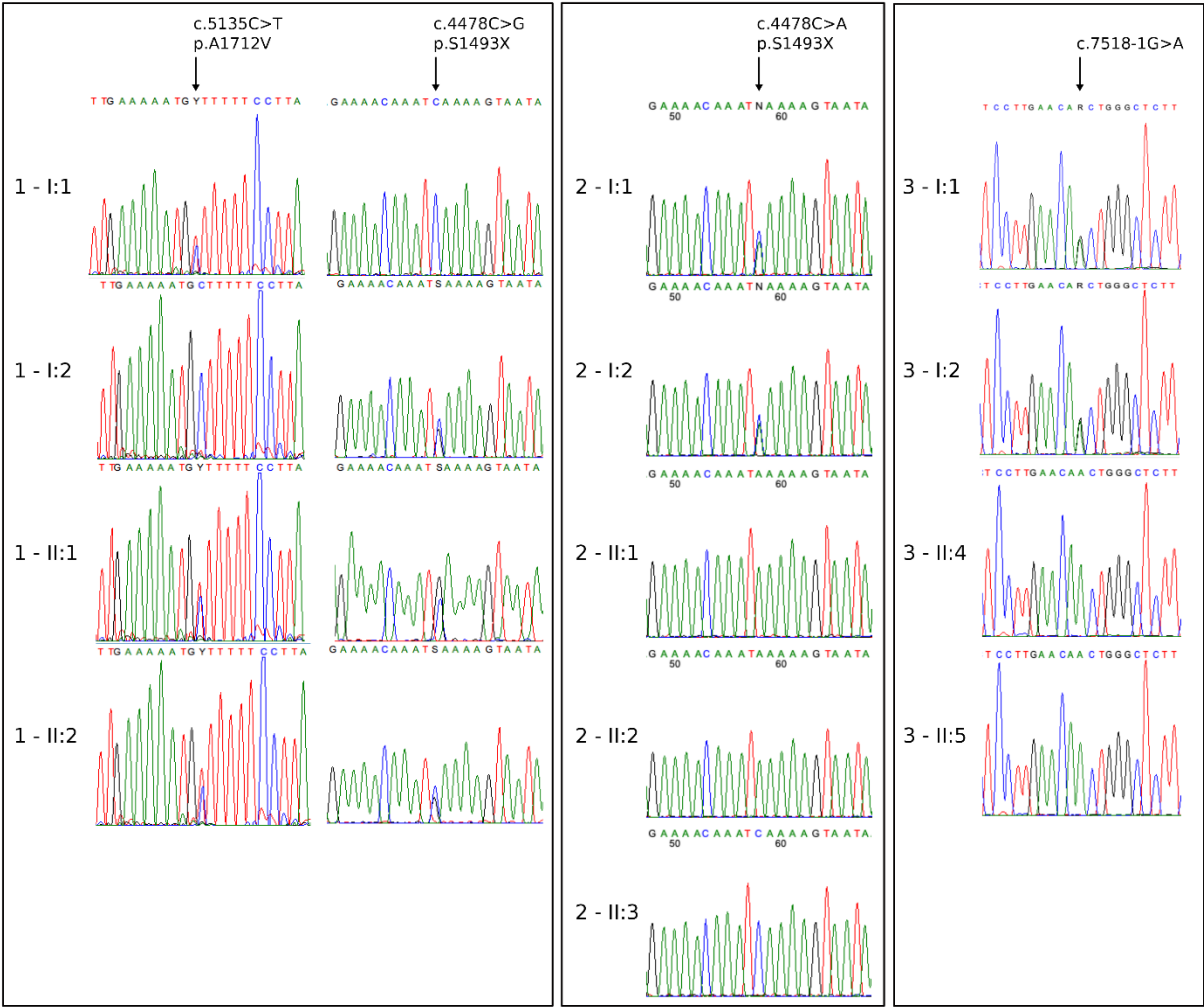
Genomic Coordinates (hg19)	<i>DMXL2</i> exon (according to NM_015263.3)	Primer Forward 5'-3'	Primer Reverse 5'-3'
chr15:g.51757849C>T	exon 31	TTGTAAAGAGAAACTTGACGGC	TTTTCTGGGTTGGAGAGTGG
chr15:g.51780233G>A	exon 22	CGACCTGGTTCCTTTAGCTG	CCTCTACAACCTTCTTAGGTTTTCAAT
chr15:g.51790943G>C	exon 18	AGAATTGATGGATTTAGGGAAAG	GGCCTCAACCGTCTTTTCTA
chr15:g.51790943G>T	exon 18	AGGAACATCTGCTCCAAACG	CCAGGATATACCAACGGATGA



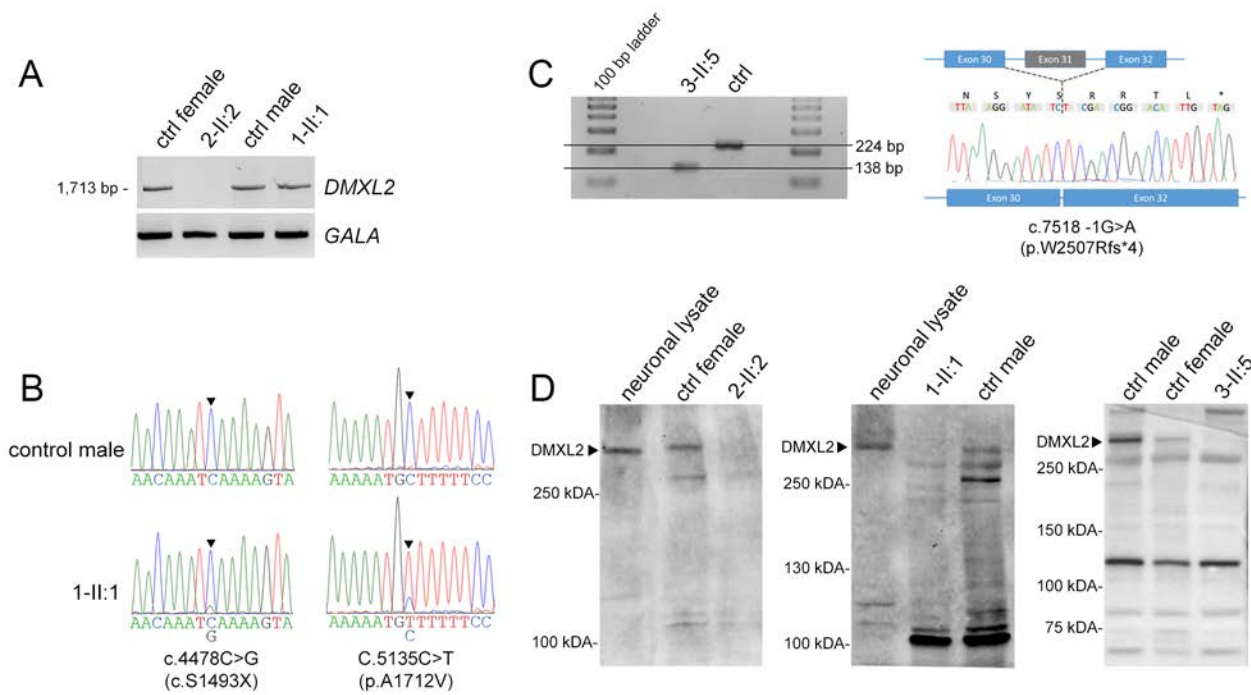
Supplementary Figure 1. Dysmorphic features in patients carrying *DMXL2* mutations. Clinical photographs of Patients 1-II:1 at four years (A) and 1-II:2 at three months (B) showing a hypotonic, flat posture. Facial photographs of Patients 1-II:1 at four years (C), 2-II:1 at one month (D), and 2-II:2 at 8.5 years (E) showing mild downslanting of palpebral fissures, epicanthal folds, short forehead, and saddle nose.



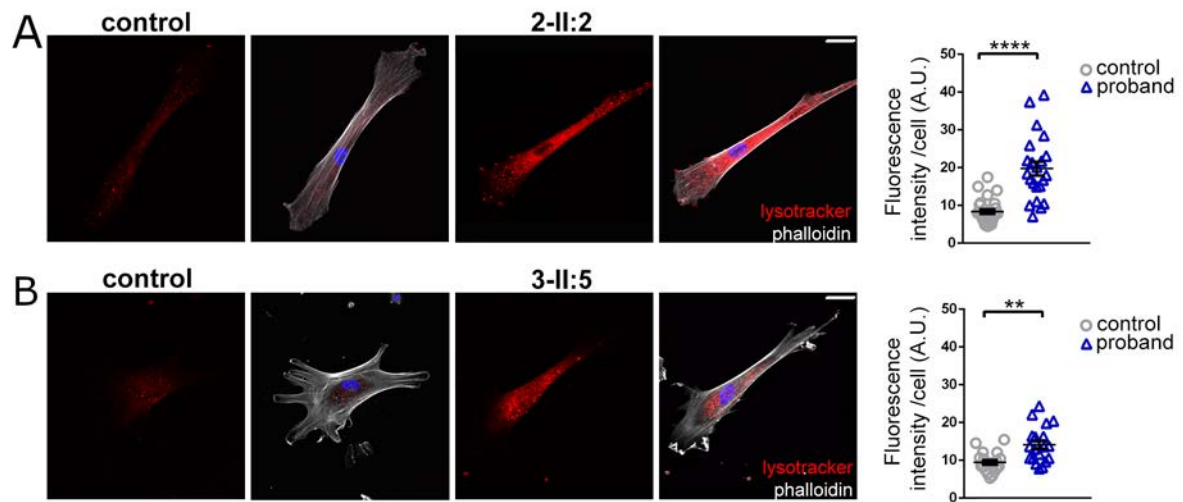
Supplementary Figure 2. Muscle biopsy in patient I-II:1. **A)** Hematoxylin-Eosin staining (magnification 20x) showing fibre cells normal for age in size and morphology. **B)** Modified Gomori Trichrome staining (magnification 20x). Neither ragged red fibres nor sarcoplasmic inclusions were detected. **C)** ATPase staining performed at pH 4.3 (magnification 20x) showing normal pattern of distribution between type 1 (dark) and type 2 (white) muscle fibres without grouping or predominance. **D)** Cytochrome C oxidase (COX) histochemistry (magnification 20x). Although present, COX reaction appeared weak in most fibres, with dotted appearance. **E)** Oil red O (ORO) staining (magnification 32x) showing increased lipid amount in sarcoplasm (red dots). **F)** Nile red fluorescent staining (magnification 40x) confirming the presence of numerous fibres filled with Nile red positive lipid droplets.



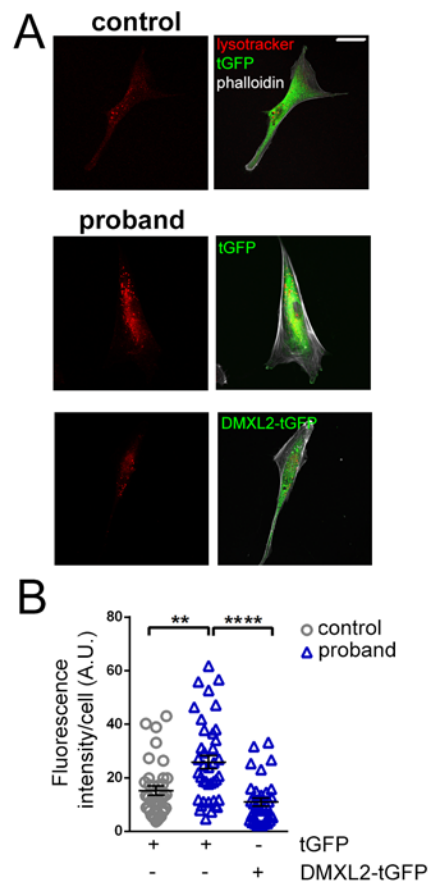
Supplementary Figure 3. Electropherograms obtained for validating segregation analysis in the three families.



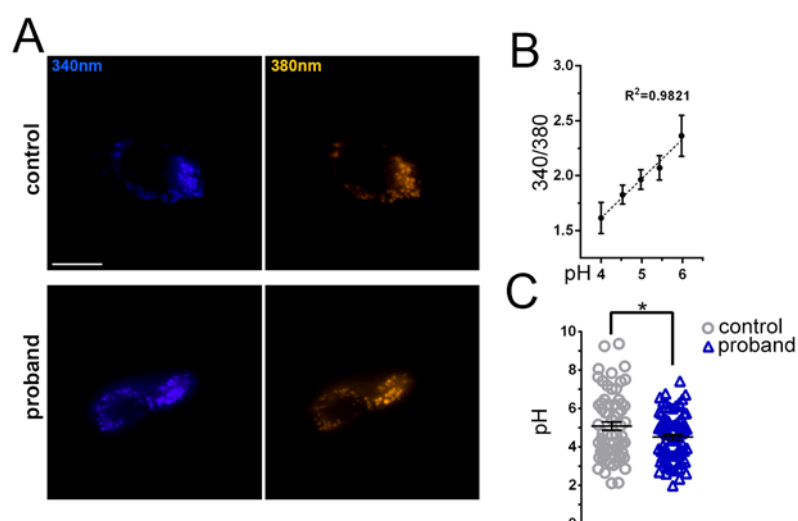
Supplementary Figure 4. (A) RT-PCR analysis of *DMXL2* in skin fibroblasts from Patients 2-II:2 and 1-II:1 compared to age- and sex-matched controls. We failed to amplify *DMXL2* cDNA in Patient 2-II:2, harboring the homozygous nonsense mutation c.4478C>A. *GALA* (alpha-galactosidase enzyme) was amplified as internal control. (B) Electropherograms of c.4478C>G and c.5135C>T mutant alleles amplified on cDNA of Patient 1-II:1 and respective control. The genomic mutation c.4478C>G, leading to the nonsense p.S1493X, is virtually undetectable in the patient's cDNA, suggesting the degradation of the mutated mRNA. Accordingly, the c.5135C>T change was present almost at the homozygous state, further confirming the degradation of the c.4478C>G transcript. (C) *Left panel*: PCR and gel electrophoresis of cDNA from Patient 3-II:5's skin fibroblasts. Primers were designed to evaluate the effect of the splice site variant c.7518-1G>A. The picture shows a single lower band in the patient compared to a control sample, indicating a shorter transcript. *Right panel*: Sanger Sequencing of the PCR product. As illustrated, the variant leads to skipping of Exon 31 resulting in a frameshift and in introduction of a premature stop codon. (D) Full-length blots of the samples presented in Fig. 1A, with positive control (neuronal lysate from primary mouse cortical neurons) for *DMXL2* identification.



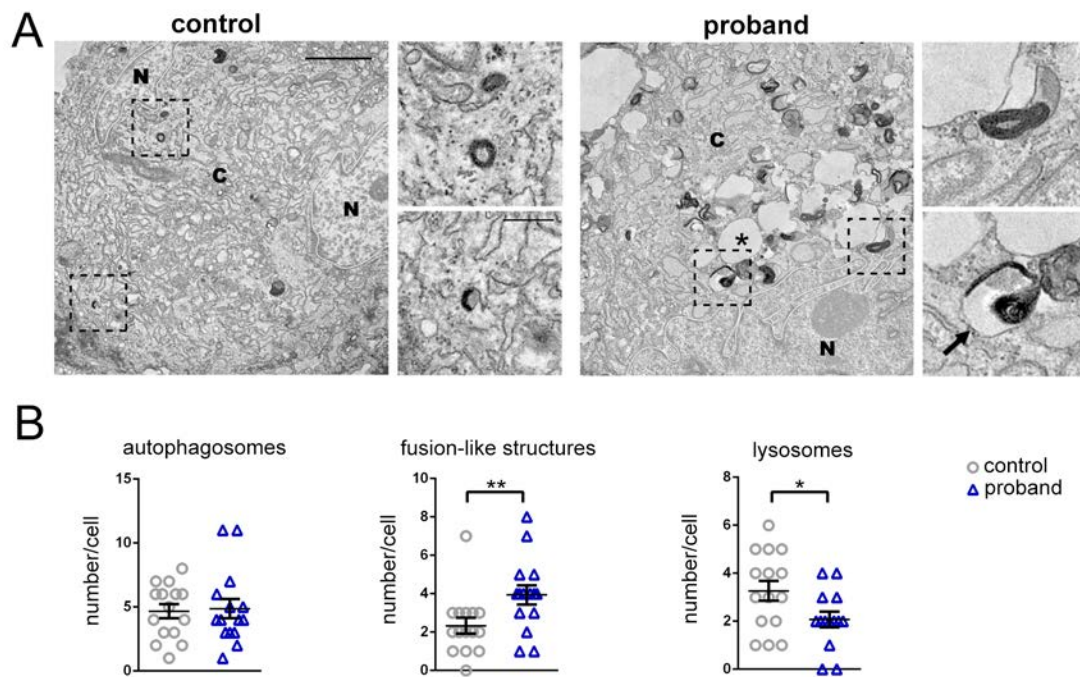
Supplementary Figure 5. Intracellular acidic organelles in patients 2-II:2 and 3-II:5 fibroblasts. (A) *Left panels:* Representative images of skin fibroblasts from Patient 2-II:2 and the respective control incubated with Lysotracker (200 nM, 1 h) and immunolabeled with phalloidin. Scale bar, 40 μ m. *Right panel:* Lysotracker fluorescence intensity (individual data and means \pm SEM) was quantified in 27 (control) and 22 (proband) cells. (B) *Left panels:* Representative images of Patient 3-II:5's skin fibroblasts and the respective control treated as in 'A'. Scale bar, 40 μ m. *Right panel:* Lysotracker fluorescence intensity (individual data and means \pm SEM) was quantified in 19 cells for each condition. ** $p < 0.01$, **** $p < 0.0001$, unpaired t -test with Welch's correction. A.U. arbitrary units of fluorescence intensity.



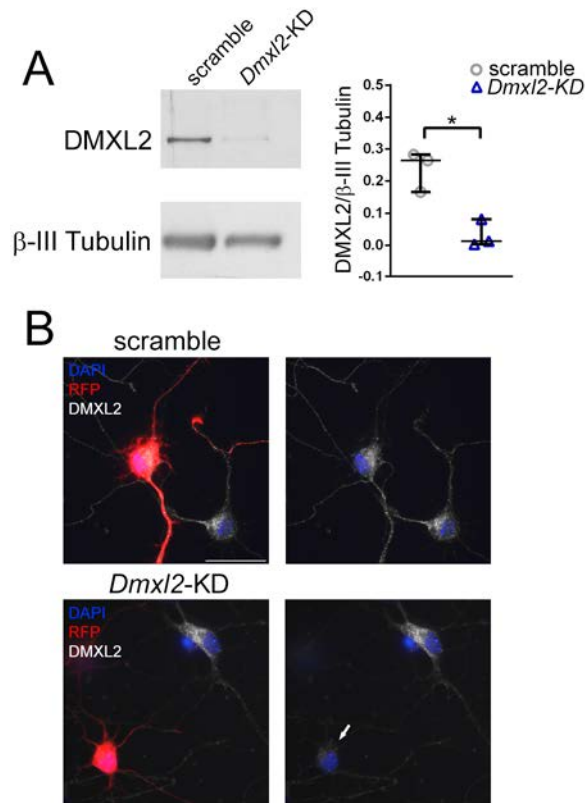
Supplementary Figure 6. Exogenous DMXL2 rescues lysotracker phenotype in Patient 1-II:1's (proband) fibroblasts. (A) Representative images of control and Patient's fibroblasts transfected with the turboGFP (tGFP) or DMXL2-tGFP vectors and incubated with Lysotracker (200nM, 1 h) and stained with phalloidin. Scale bar, 40μm (B) Lysotracker fluorescence intensity (individual data and means ± SEM) was quantified in 36 (control), 39 (proband + tGFP) cells and 36 (proband + DMXL2-tGFP). **p<0.01; **** p<0.0001, Kruskal-Wallis/Dunn's tests.



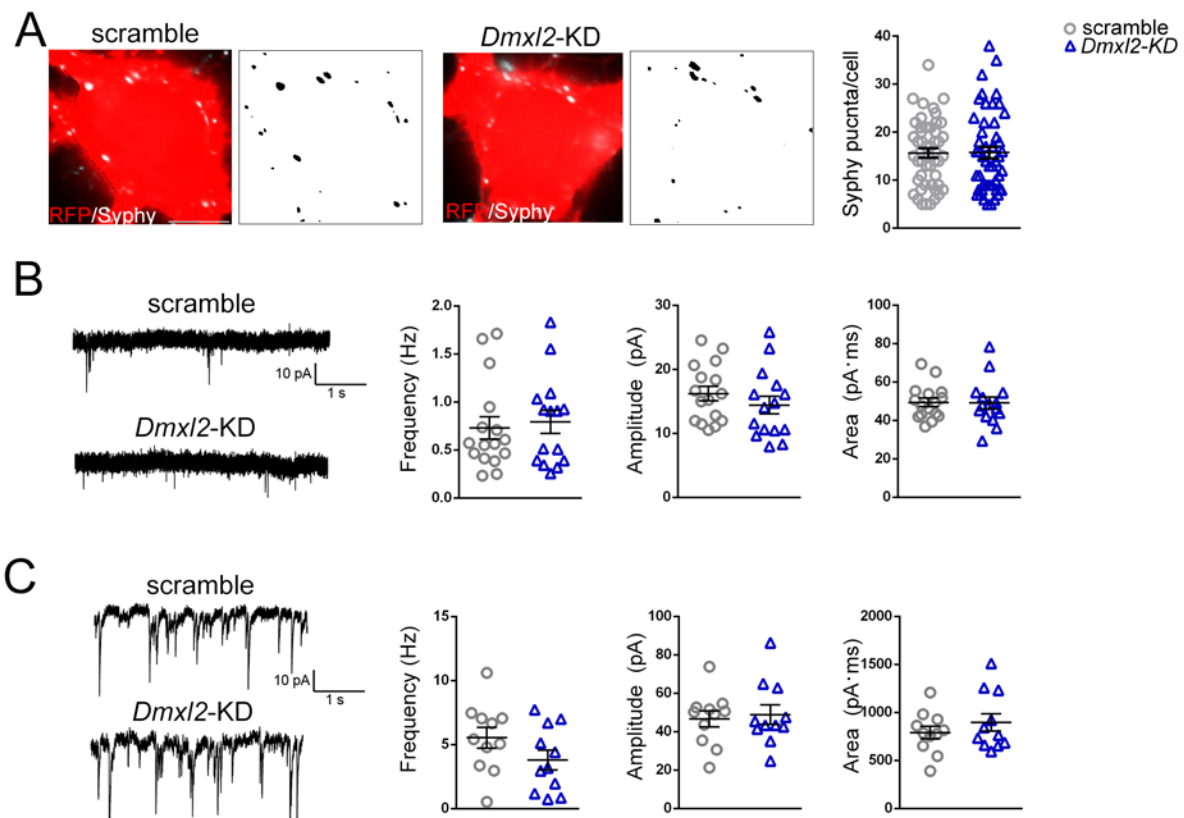
Supplementary Figure 7. Measurement of intracellular organelle pH. (A) Representative images showing control and Patient 1-II:1's (proband) skin fibroblasts treated with LysoSensor Yellow/Blue DND-160. Scale bar, 20 μ m. (B) Graph showing the calibration curve generated to calculate intracellular pH. Data are means \pm SEM from 5 independent measures. (C) Quantification of pH values in control and proband's fibroblasts calculated from the 340/380nm ratio interpolation in the calibration curve. Data are means \pm SEM from 65 and 73 cells from control and proband's fibroblasts respectively. * $p < 0.05$, unpaired t -test with Welch's correction.



Supplementary Figure 8. Transmission electron microscopy (EM) in and patient 1-II:1's (proband) fibroblasts. (A) Representative TEM micrographs of cultured fibroblasts from control and Patient 1-II:1 (proband) (scale bar, 2 μ m). Dotted squares indicate high magnifications shown on the right. The arrow indicates atypical fusion-like structures and the asterisk indicates vacuolization. (B) Quantitative analysis of autophagosomes, fusion-like structures and lysosomes. Data are means \pm SEM of 15 cells for experimental condition. * $p < 0.05$, ** $p < 0.01$ unpaired Student t -test with Welch's correction and Mann Whitney U -test.



Supplementary Figure 9. Efficacy of *Dmxl2* knockdown by RNA interference. (A) Representative western blot showing DMXL2 expression in mouse hippocampal neurons 7 days after nucleofection with scramble or *Dmxl2*-shRNA (*Dmxl2*-KD). β -III Tubulin is shown for equal loading. Densitometric quantification is shown on the right. Data are means \pm SEM from three independent preparations. *p<0.05, Mann-Whitney unpaired *t*-test. (B) Representative images of mouse hippocampal neurons transfected at 4 DIV with scramble or *Dmxl2*-shRNA and immunostained for DMXL2 at 7 DIV. DMXL2 signal is present in not-transfected and scramble transfected neurons but not detectable in protein is not detectable in *Dmxl2*-KD neuron (arrow). Scale bar, 30 μ m.



Supplementary Figure 10. Somatic synapses and miniature postsynaptic currents in *Dmxl2* silenced neurons. (A) *Left panels*: High magnification of somatic Synaptophysin (Syphy) staining in 17 DIV hippocampal neurons transfected at 14 DIV with either control shRNA (scramble) or *Dmxl2*-shRNA (*Dmxl2*-KD) harbouring the Red Fluorescent Protein (RFP). Thresholded Syphy signals are shown on the right. Scale bar, 5 μ m. *Right panel*: Quantitative analysis of somatic synaptic contacts. Data are means \pm SEM of 49 neurons per experimental condition, from three independent preparations. (B) *Left panels*: Representative traces of miniature excitatory postsynaptic currents (mEPSCs) recorded at -70 mV from 17 DIV hippocampal neurons in the both experimental conditions. *Right panels*: Frequency, amplitude and area of mEPSCs recorded in control (n=16) and *Dmxl2*-KD (n=15) neurons from three independent preparations. (C) *Left panels*: Representative traces of miniature inhibitory postsynaptic currents (mIPSCs) recorded at -70 mV from 17 DIV hippocampal neurons in both experimental conditions. *Right panels*: Frequency, amplitude and area of mIPSCs recorded in control (n=11) and *Dmxl2*-KD (n=11) neurons from two independent preparations.

Supplementary References

- Abecasis GR, Cherny SS, Cookson WO, Cardon LR. Merlin--rapid analysis of dense genetic maps using sparse gene flow trees. *Nat. Genet.* 2002; 30: 97–101.
- DePristo MA, Banks E, Poplin R, Garimella K V., Maguire JR, Hartl C, et al. A framework for variation discovery and genotyping using next-generation DNA sequencing data. *Nat. Genet.* 2011; 43: 491–8.
- Kremer LS, Bader DM, Mertes C, Kopajtich R, Pichler G, Iuso A, et al. Genetic diagnosis of Mendelian disorders via RNA sequencing. *Nat. Commun.* 2017; 8: 15824.
- Li H, Durbin R. Fast and accurate short read alignment with Burrows-Wheeler transform. *Bioinformatics* 2009; 25: 1754–60.
- Li H, Handsaker B, Wysoker A, Fennell T, Ruan J, Homer N, et al. The Sequence Alignment/Map format and SAMtools. *Bioinformatics* 2009; 25: 2078–9.
- McKenna A, Hanna M, Banks E, Sivachenko A, Cibulskis K, Kernytzsky A, et al. The Genome Analysis Toolkit: a MapReduce framework for analyzing next-generation DNA sequencing data. *Genome Res.* 2010; 20: 1297–303.
- Smith KR, Bromhead CJ, Hildebrand MS, Shearer AE, Lockhart PJ, Najmabadi H, et al. Reducing the exome search space for mendelian diseases using genetic linkage analysis of exome genotypes. *Genome Biol.* 2011; 12: R85.
- Thorvaldsdóttir H, Robinson JT, Mesirov JP. Integrative Genomics Viewer (IGV): high-performance genomics data visualization and exploration. *Brief. Bioinform.* 2013; 14: 178–92.
- Van der Auwera GA, Carneiro MO, Hartl C, Poplin R, Del Angel G, Levy-Moonshine A, et al. From FastQ data to high confidence variant calls: the Genome Analysis Toolkit best practices pipeline. *Curr. Protoc. Bioinforma.* 2013; 43: 11.10.1-33.
- Wang K, Li M, Hakonarson H. ANNOVAR: Functional annotation of genetic variants from high-throughput sequencing data. *Nucleic Acids Res.* 2010; 38: 1–7.